PCCP

Amorphous graphene: A constituent part of low density amorphous carbon

Journal:	*Physical Chemistry Chemical Physics*
Manuscript ID	CP-ART-04-2018-002545.R2
Article Type:	Paper
Date Submitted by the Author:	04-Jul-2018

Complete List of Authors:	Bhattarai, Bishal; Ohio University, Dept. of Physics and Astronomy Biswas, Parthapratim; University of Southern Mississippi College of Science and Technology Atta-Fynn, Raymond; University of Texas Arlington College of Science, Department of Physics and Astronomy Drabold, David; Ohio University, Dept. of Physics and Astronomy

Physical Chemistry Chemical Physics

ARTICLE TYPE

Cite this: DOI: 10.1039/xxxxxxxxxx

Amorphous graphene: A constituent part of low density amorphous carbon†

Bishal Bhattarai,[a] Parthapratim Biswas,[b] Raymond Atta-Fynn,[c] and D. A. Drabold*[d]

Received Date
Accepted Date

DOI: 10.1039/xxxxxxxxxx

www.rsc.org/journalname

In this paper, we provide evidence that low density nano-porous amorphous carbon (a-C) consists of interconnected regions of amorphous graphene (a-G). We include experimental information in producing models, while retaining the power and accuracy of *ab initio* methods with no biasing assumptions. Our models are highly disordered with predominant sp^2 bonding and ring connectivity mainly of sizes 5-8. The structural, dynamical and electronic signatures of our 3-D amorphous graphene is similar to the monolayer amorphous graphene. We predict an Extended X-ray Absorption Fine Structure (EXAFS) signature of amorphous graphene.Electronic density of states calculations for 3-D amorphous graphene reveal similarity to monolayer amorphous graphene and the system is not conducting.

1 Introduction

Amorphous graphene (a-G): an idealized 2-D structure consisting of 5-6-7 polygons with predominant sp^2 bonding has presented a challenge for extraction. This has been achieved by exposure of an of electron beam to a crystalline/pristine graphene (p-graphene) sheet, to produce an amorphous monolayer.[1] Similarly, a-G has been modeled by introducing 5 and 7 member rings with a *Wooten-Weaire-Winer* (WWW) scheme.[2–5]

Advancement and understanding of amorphous materials has been limited by conventional simulations.[6] A generic approach: "*melt quenching*"(MQ) via molecular dynamics (MD), is limited by quenching rate, and model size (for *ab initio* interactions). Meanwhile, MQ models prepared using inter-atomic potentials directly depends upon the choice of inter-atomic interactions. A recent work of *Li et. al.* has highlighted this by comparing models of amorphous carbon prepared using Tersoff, REBO, ReaxFF potential. Alternatively, tight-binding molecular-dynamics (TBMD)[7] and its hybrid modifications[8] are also used as an efficient alternative to model amorphous solids. In contrast, high-precision experimental data from diffraction, infrared (IR), and nuclear magnetic resonance (NMR) are readily available. The reverse monte carlo (RMC) method is used to determine the structure of complex materials by inverting experimental diffraction data. This method often leads to unsatisfactory and unphysical results, as scattering data lack sufficient information to uniquely resolve local structural features. This difficulty in inversion of experimental data has led to several attempts with multiple experimental constraints which is a difficult optimization problem and use of hybrid schemes of RMC.[9–12] Hybrid methods incorporates an additional penalty function based on force fields to the conventional structural refinement of RMC method. Several variations and implementation of these hybrid approaches has been discussed elsewhere. In this work we have used a recently developed hybrid approach FEAR (Force Enhanced Atomic Refinement) method, an *ab initio* structural refinement technique, to provide clear evidence that low density phases of Carbide-Derived Carbons (CDC)[13–16] are a form of three dimensional a-G (warped, wrapped 2D a-G sheets with ring disorder and defects).

FEAR is a means to invert diffraction data and simultaneously determine coordinates at a suitable *ab initio* energy minimum, starting from a random configuration. FEAR is an efficient and robust method to model different amorphous systems. It has been so far successfully applied to a-Si, a-SiO_2, Ag-doped $GeSe_3$ and a-C at various densities.[17–20] For the case of amorphous silicon FEAR has been successfully implemented for up to 1024 atoms.[21]

2 Methodology and models

To tersely recapitulate FEAR, we begin with some definitions. If $V(X_i....X_n)$ is the energy functional for atomic coordinates $\{X_i\}$ and χ^2 measures the discrepancy between (say) a diffraction experiment and computer model, we seek to find a set of atomic coordinates $\{X_i\}$ with the property that $V = minimum$ and χ^2 is within experimental error. FEAR consists of (i) producing a ran-

[a] *Department of Physics and Astronomy, Condensed Matter and Surface Science Program (CMSS), Ohio University, Athens, Ohio 45701, USA.*
[b] *Department of Physics and Astronomy, The University of Southern Mississippi, Hattiesburg, Mississippi 39406, USA.*
[c] *Department of Physics, University of Texas, Arlington, Texas 76019, USA.*
[d] *Department of Physics and Astronomy, Nanoscale and Quantum Phenomena Institute (NQPI), Ohio University, Athens, Ohio 45701, USA.*

† Electronic Supplementary Information (ESI) available: [Computational details of FEAR and comparison]

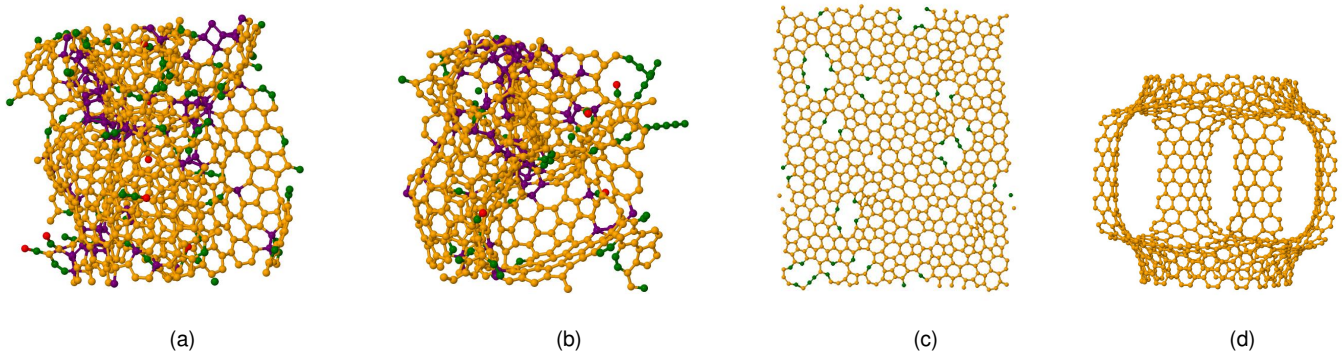

Fig. 1 Structure models: (a) 3-D a-graphene (800 atom), (b) 3-D a-graphene (648 atom) (c) 2-D a-graphene[4], and (d) 3-D schwarzite.[22] color coding: purple (sp^3), orange (sp^2), green (sp) and red (singly bonded).

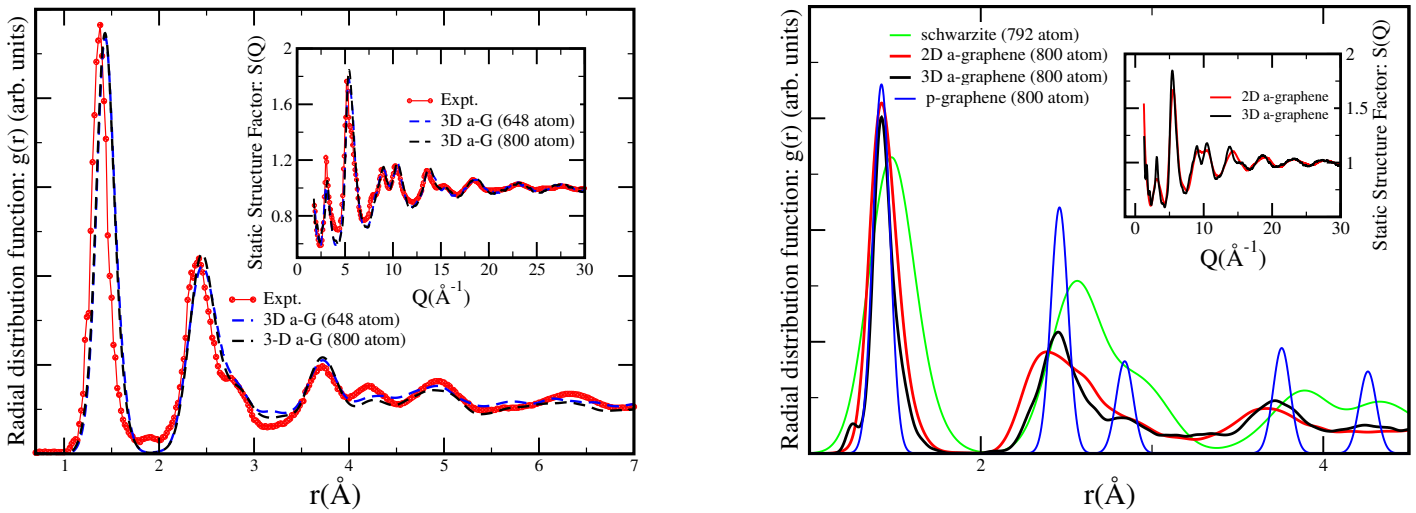

Fig. 2 (Left panel) Comparison of radial distribution function $g(r)$ and structure factor ($S(Q)$, inset) of FEAR models with experiment($\rho = 0.95\ g/cm^3$).[23] **(Right panel)** Radial distribution functions $g(r)$ of four models (3-D a-graphene (800 atom), 2-D a-graphene (800 atom), crystalline/pristine graphene (p-graphene, 800 atom) and schwarzite (792 atom)), **(inset)** Comparison of static structure factor $S(Q)$ between 3-D and 2-D a-graphene.

dom structural model at an assumed density, (ii) invoking N accepted moves with Reverse Monte Carlo (RMC) followed by M conjugate-gradient (CG) relaxation steps using *ab initio* interactions. We then iterate (ii) to convergence (fitting the experimental data and finding a suitable minimum of DFT interactions). Accurate and unbiased chemical information is included in the CG step.

In this paper, a *random* starting configuration is employed along with the code RMCProfile[24] with values of $M = 1$ and $N \sim 100$ respectively. We have used silicon carbide-derived nanoporous carbon (SIC-CDC)[23] at density 0.95 g/cm^3 as our ex-perimental data. We have used a maximum RMC step size of 0.15-0.375 $\AA$, restricting minimum approach distance between atoms to 1.05 $\AA$, a fixed spacing of 0.02 $\AA$ and 0.04 weight of the exper-imental data. The relaxation step was performed with single-ζ basis, periodic boundary conditions and Harris functional at con-stant volume using DFT code SIESTA.[25] Finally, we relax con-verged models using Vienna *ab initio* package (VASP).[26–30] All the calculations were performed with a single k-point $\Gamma(\vec{k} = 0)$ and the local density approximation, and PAW potentials. We started with random initial configurations, and made FEAR models with 216, 648 and 800 atoms. We observe in passing that FEAR is computationally highly advantageous compared to MQ, requiring far fewer calls to the *ab initio* code (in the FEAR CG step). We explore reproducibility with models containing 216, 648 and 800 atoms, and show that a consistent network topology emerges.

To explain and interpret the results, we have created MQ models with 648 and 216 atoms. The 648-atom MQ model was equilibrated at 7000 K, then cooled to 300 K, and after further equilibration at 300 K, was relaxed using the CG method. This process required 50 ps of total simulation time. Due to the large size of the system we have used the DFT code SIESTA with Harris functional to form this model. We also have created a 216-atom MQ model with the help of plane wave DFT code VASP, using the local-density approximation with Ceperley-Alder (CA) exchage correlation functional. The VASP model was first equilibrated at 7500 K, then quenched to 300K in multiple steps over a total simulation time of 42 ps using a time step of 2 fs. A plane wave cut off of 350 eV and energy difference criteria of 10^{-4} was chosen for the simulation. These are typical simulation times used

in preparing accurate models of amorphous systems* Additionally, we discuss crystalline/pristine graphene (**p-graphene**, 800 atoms)[4] and a schwarzite model (792 atoms)[22] for comparison. The details are summarized in (Table 1, **ESI**†).

3 Results and discussion

In Fig. 1, we show the topology of our models. sp^2 bonding (in orange) dominates each of these structure. 3-D amorphous graphene has a few sp^3 bonded sites ($\sim 11\%$) which mainly connect one sp^2 graphene fragment to another. Similarly, a few sp bonded sites appear in both 3-D and 2-D amorphous graphene. In Fig. 2(left panel), we compare our results with the experimental results of nano-porous Silicon Carbide Derived Carbon (SiC-CDC) at density 0.95 g/cm^3.[23] We observe good agreement with the experiment (by construction) while a slight deviation is observed upon complete *ab initio* (VASP) relaxation. We have plotted the radial distribution function $g(r)$ for the four models and the static structure factor $S(Q)$ in Fig. 2(right panel). 3-D a-graphene model has first nearest-neighbor distance at 1.42 $\AA$ and second nearest-neighbor distance at 2.45 $\AA$ same as crystalline graphene model. Meanwhile, the 2-D a-graphene model[3,4] reveals a second peak in $g(r)$ with second nearest-neighbor at 2.38 $\AA$, suggesting a broader distribution bond-angles than 3-D a-graphene model[7] (see Fig. 3(right panel)).

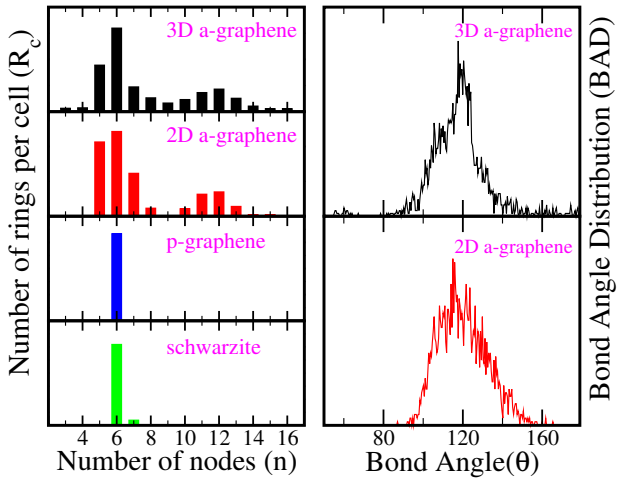

Fig. 3 Comparison of ring distribution between the four models and plot of bond-angle distribution of 3-D and 2-D a-graphene.

Both 2-D and 3-D a-graphene exhibit bond angle distribution (BAD) with peak around $\sim 120^o$. The full width at half maximum of BAD has a value of 27.45^o and 26.65^o for 2-D and 3-D graphene respectively. It is observed that with high sp^2 concentration, BAD is around 117.0^o.[34] The plot of static structure factor $S(Q)$ for 2-D and 3-D a-graphene shows a striking similarity between these structures. We obtain similar structures with melt-quench approach with *ab initio* code VASP (Fig. 1 and Table 1, **ESI** †).

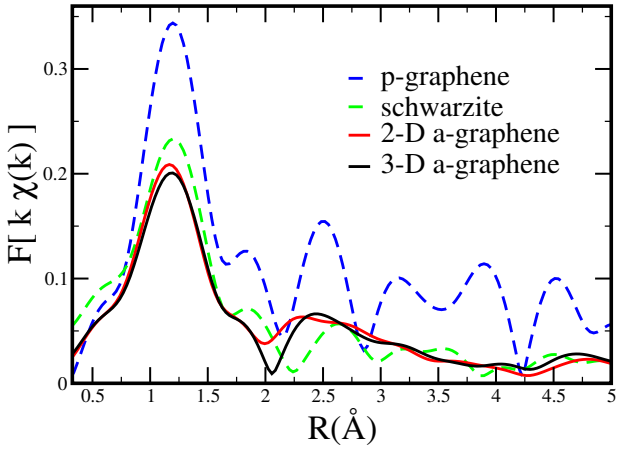

Fig. 4 Fourier transform of Carbon K-edge EXAFS spectra [$k\chi(k)$] for the four models.

In Fig. 3, the ring distribution shows that both 2-D and 3-D a-graphene have ring structures of various sizes (mostly 5, 6 and 7), as in shungite.[35] In contrast, both schwarzite and p-graphene exhibit 6-membered rings (exception: schwarzite has few 7-membered rings). We have also computed Extended X-ray Absorption Fine Structure (EXAFS) for our four models (see Fig. 4). EXAFS is valuable for the first-shell information.[36] We observe strong structural correlation of 3-D graphene and 2-D graphene in our EXAFS plot,[37,38] whereas pristine graphene and schwarzite structures distinctively differ from these structures. We show an EXAFS signatures differentiating 2-D and 3-D a-G (a peak at $\sim$ 2.2 $\AA$, see Fig. 4).

The electronic density of states (EDOS) and vibrational density of states (VDOS) are reported next. The low energy modes are related to mechanical properties and low temperature thermal conductivity of a material.[39–42] The force constant matrix was obtained from a finite difference method displacing every atom in 6-directions ($\pm x$,$\pm y$,$\pm z$) with a small displacement of 0.015 cm^{-1}. The first three frequencies arising due to supercell translations which are very close to zero are neglected in our calculation and all our other frequencies are positive (no imaginary modes). Once again due to gigantic size of our model we have Harris functional to our advantage with a double-ζ basis (see details[31,43]). Our 3-D amorphous graphene shows two distinctive components in VDOS (Fig. 5 (left panel)). A sharp peak around ~ 814 cm^{-1} and a broader peak at ~ 1300 cm^{-1}, and a narrow neck is observed at ~ 470 cm^{-1}. We have an surprising match of VDOS for our model and 2-D amorphous graphene. The VDOS for crystalline graphene and schwarzite reveal a different profile to amorphous graphene. The pristine graphene VDOS peaks are observed at: ~ 490 cm^{-1}, ~ 678 cm^{-1} and ~ 1460 cm^{-1}, with peak intensities and position

* It is worth noting that melt-quench (MQ) process does depends on cooling rate. However, our earlier study done for several models of amorphous carbon at different cooling rates showed only slight differences in bonding (sp, sp^2 and sp^3) preferences without much change in other observables such as electronic density of states or vibrational properties.[31] Recently it has been shown that very slow quenching rate improves the quality of MQ models.[32,33] These simulations are very extended and do not seem to be an efficient way to model amorphous systems. FEAR produces models with DFT accuracy taking less CPU time. Computationally speaking, our 216 atom FEAR model presented here requires 1/14 the time used for the 216 atom VASP (MQ) model (Table 1, **ESI**†) and requires total force calls of ($\sim 6000 - 8000$) to obtain a converged model.

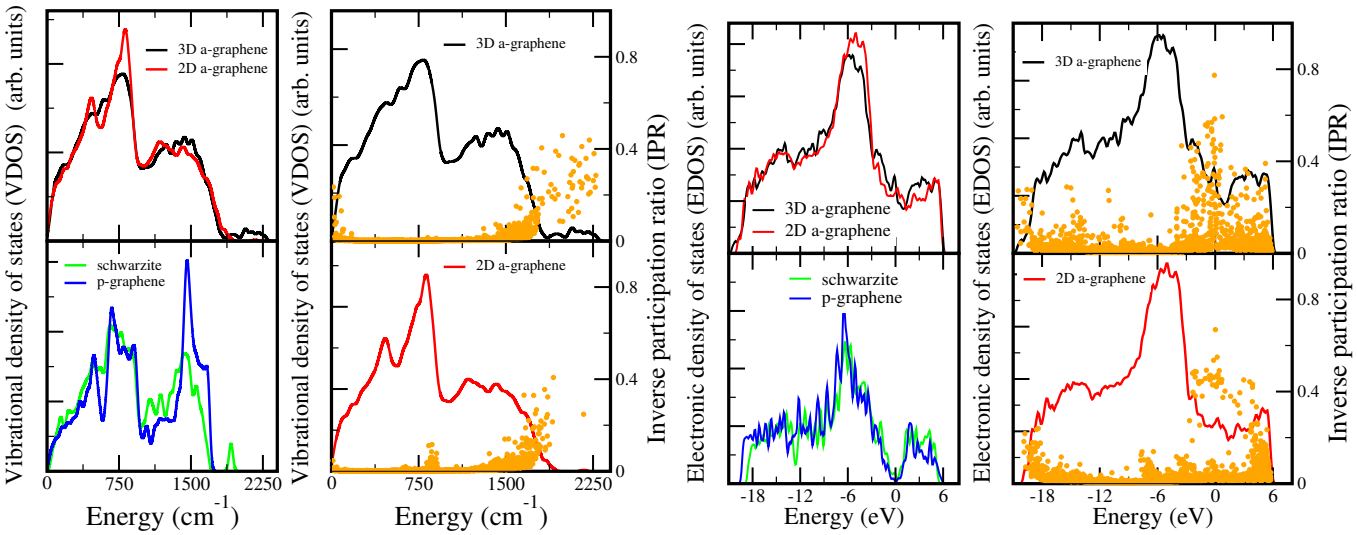

Fig. 5 (Left panel) Plot and comparison of vibrational density of states for the four models. The 3-D graphene (a-carbon) has excellent similarity with the 2-D a-graphene. The yellow dot represent vibrational inverse participation ratio (IPR, equation (1)). **(Right panel)** Plot and comparison of EDOS (E_F=0 eV) and localization (IPR, yellow dot, equation (2)).

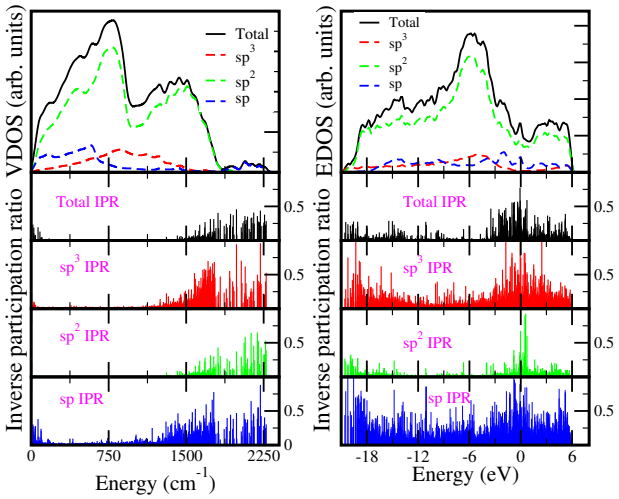

Fig. 6 (Left panel) Plot of Total, (sp^3, sp^2, sp) projected VDOS and vibrational IPR for 3-D a-graphene model. **(Right panel)** Plot showing Total, (sp^3, sp^2, sp) projected EDOS and electronic IPR for the 3-D a-graphene model.

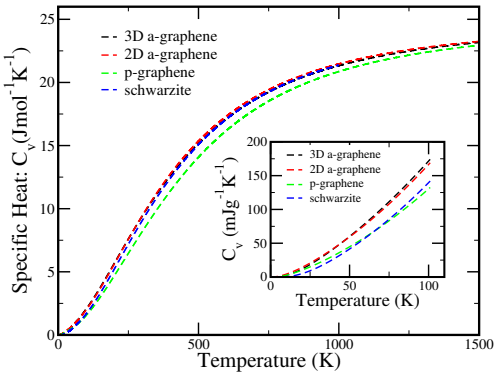

Fig. 7 Specific heat plots for the four models. (**Inset**) Low temperature specific heat of the four models.

quite different to amorphous graphene. We associate the peak at $\sim 814\ cm^{-1}$ with a-graphene and a peak around $\sim 1460\ cm^{-1}$ for p-graphene as signature peaks.

In Fig. 5 (right panel), we report the EDOS for these four models. The EDOS for both 3-D and 2-D graphene exhibit a striking similarity, and various defects (sp^3 and sp) and topology seem to have modest effect. A similar observation was also seen in ZrC-CDC structure.[14] Separate computations (not shown here) are in agreement with previously established result of *Van Tuan et. al.*[44] which showed that these materials are not conducting. We note that the EDOS of crystalline graphene and schwarzite are quite distinct from its amorphous counterpart. We define the inverse participation ratios for vibrations and electrons as:

$$\mathscr{I} = \frac{\sum_{i=1}^{N} |u_i^j|^4}{\left(\sum_{i=1}^{N} |u_i^j|^2\right)^2} \qquad (1) \qquad \mathscr{I}(\psi_n) = \frac{\sum a_i{}^4}{\left(\sum a_i{}^2\right)^2} \qquad (2)$$

Where, (u_i^j) is normalized eigenvector of j^{th} mode and a_i are the components of eigenvector projected onto atomic s, p, and d states.

The electronic and vibrational states of amorphous solids are affected by disorder present in the structure. The localization of electronic/vibrational states can be quantified by computing inverse participation ration (IPR).[45] A completely localized state would have an IPR value unity while an extended state has a value of $(1/N)$ i.e. distributed over N atoms. Vibrational IPR is evaluated using obtained normalized displacement vectors (u_i^j) as shown in equation (1).[46] Similarly, localization of n^{th} electronic state is computed as shown in equation(2), where a_i are the components of eigenvector projected onto atomic s, p and d states (obtained from VASP).[45,47] By comparison of the localization of

states for both 2D and 3D a-graphene near Fermi energy, we see mostly extended states with few weakly localized states. We again obtain that the vibrational modes are mostly extended, with few localized modes around $\sim 1800-2000\ cm^{-1}$. We further dissect the VDOS and EDOS into sp, sp^2 and sp^3 contributions to gain further insight into 3D a-graphene model (Fig. 6). The decomposed VDOS shows that sp^2 bonding clearly dominates the vibrational spectrum. Further, we can clearly observe the narrow neck at $\sim 470\ cm^{-1}$, seen in 2D a-G. We further decompose the vibrational localization into sp, sp^2 and sp^3 components. Most localization in this system is contributed by sp and sp^3 bond. Decomposition of EDOS into sp, sp^2 and sp^3 contributions shows quite an interesting result. The sp and sp^3 bonding atoms have almost no effect on the electronic properties both at conduction band or deep into valance band. Similar to VDOS, most of the electronic localization in due to sp and sp^3 bonded carbon networks. We have computed specific heat in the harmonic approximation, $C_v(T)$ for the four models shows similar pattern at high temperatures, with p-graphene showing slight deviation compared to other models (see Fig. 7). The inset shows more prominent changes at the lower temperatures (0 K to 100 K). The two amorphous graphene models (2-D and 3-D) increases with same slope between 0 K to 100K. Meanwhile, a deviation from a-graphene is seen for the case of p-graphene and schwarzite.

4 Conclusions

In summary, we have shown that a-C with density $0.95\ g/cm^3$ is a form of a-G. We provide a detailed analysis of our model by computing structural, vibrational and electronic properties and comparing to 2D amorphous graphene along with other sp^2 structures. Surprisingly, bonding defects ($\sim 11\%\ sp^3$ and $\sim 11\%\ sp$) have little effect on properties like the EDOS and VDOS.

Conflicts of interest

There are no conflicts to declare.

Acknowledgements

We thank Prof. Michael Treacy and particularly Dr. Ronald Cappelletti for helpful conversations. We thank the Ohio Supercomputer Center and NVIDIA Corporation for, supercomputer time and a Tesla K40 GPU donation, respectively. We acknowledge US NSF grant under numbers: DMR 1506836, 1507118, 1507670 and 1507166. DAD thanks Prof. S. R. Elliott and Trinity College for hospitality.

Notes and references

1 J. Kotakoski, A. V. Krasheninnikov, U. Kaiser and J. C. Meyer, *Phys. Rev. Lett.*, 2011, **106**, 105505.

2 V. Kapko, D. A. Drabold and M. F. Thorpe, *physica status solidi (b)*, 2010, **247**, 1197–1200.

3 Y. Li, F. Inam, A. Kumar, M. F. Thorpe and D. A. Drabold, *physica status solidi (b)*, 2011, **248**, 2082–2086.

4 Y. Li and D. A. Drabold, *physica status solidi (b)*, 2013, **250**, 1012–1019.

5 H. Terrones, M. Terrones, E. Hernández, N. Grobert, J.-C. Charlier and P. M. Ajayan, *Phys. Rev. Lett.*, 2000, **84**, 1716–1719.

6 G. T. Barkema and N. Mousseau, *Phys. Rev. Lett.*, 1996, **77**, 4358–4361.

7 C. Z. Wang and K. M. Ho, *Phys. Rev. Lett.*, 1993, **71**, 1184–1187.

8 A. S. Sinitsa, I. V. Lebedeva, A. M. Popov and A. A. Knizhnik, *The Journal of Physical Chemistry C*, 2017, **121**, 13396–13404.

9 B. Meredig and C. Wolverton, *Nature Materials*, 2012, **12**, 123 EP.

10 P. Biswas, R. Atta-Fynn and D. A. Drabold, *Phys. Rev. B*, 2007, **76**, 125210.

11 G. Opletal, T. Petersen, B. Omalley, I. Snook, D. G. Mcculloch, N. A. Marks and I. Yarovsky, *Mol. Sim.*, 2002, **28**, 927–938.

12 A. K. Soper, *Molecular Physics*, 2001, **99**, 1503–1516.

13 A. H. Farmahini and S. K. Bhatia, *Carbon*, 2015, **83**, 53 – 70.

14 M. J. Lopez, I. Cabria and J. A. Alonso, *The Journal of Chemical Physics*, 2011, **135**, 104706.

15 L. Alonso, J. A. Alonso and M. J. Lopez, *Computer simulation of the structure of Nonporous carbons and higher density phases of carbon, in Many-body Approaches at Different Scales, a tribute to Norman H. March*, Springer, p. 21 2018.

16 C. de Tomas, I. Suarez-Martinez, F. Vallejos-Burgos, M. J. Lopez, K. Kaneko and N. A. Marks, *Carbon*, 2017, **119**, 1 – 9.

17 A. Pandey, P. Biswas and D. A. Drabold, *Scientific Reports*, 2016, **6**, 33731.

18 A. Pandey, P. Biswas and D. A. Drabold, *Phys.Rev.B*, 2015, **92**, 155205.

19 A. Pandey, P. Biswas, B. Bhattarai and D. A. Drabold, *Phys.Rev.B*, 2016, **94**, 235208.

20 B. Bhattarai, A. Pandey and D. Drabold, *Carbon*, 2018, **131**, 168 – 174.

21 D. Igram, B. Bhattarai, P. Biswas and D. Drabold, *Journal of Non-Crystalline Solids*, 2018, **492**, 27 – 32.

22 H. Terrones and M. Terrones, *New Journal of Physics*, 2003, **5**, 126.

23 A. H. Farmahini, G. Opletal and S. K. Bhatia, *The Journal of Physical Chemistry C*, 2013, **117**, 14081–14094.

24 M. G. Tucker, D. A. Keen, M. T. Dove, A. L. Goodwin and Q. Hui, *J. Phys.: Condens. Matter*, 2007, **19**, 335218(1–16).

25 J. M. Soler, E. Artacho, J. D. Gale, A. Garcia, J. Junquera, P. Ordejon and D. Sanchez-Portal, *Journal of Physics: Condensed Matter*, 2002, **14**, 2745–2779.

26 G. Kresse and D. Joubert, *Phys.Rev.B*, 1999, **59**, 1758–1775.

27 G. Kresse and J. Furthmuller, *Phys.Rev.B*, 1996, **54**, 11169–11186.

28 P. E. Blochl, *Phys.Rev.B*, 1994, **50**, 17953–17979.

29 M. Hacene, A. Anciaux-Sedrakian, X. Rozanska, D. Klahr, T. Guignon and P. Fleurat-Lessard, *Journal of Computational Chemistry*, 2012, **33**, 2581–2589.

30 M. Hutchinson and M. Widom, *Computer Physics Communications*, 2012, **183**, 1422 – 1426.

31 B. Bhattarai and D. A. Drabold, *Carbon*, 2017, **115**, 532–538.

32 V. L. Deringer, N. Bernstein, A. P. Bartók, M. J. Cliffe, R. N. Kerber, L. E. Marbella, C. P. Grey, S. R. Elliott and G. Csányi, *The Journal of Physical Chemistry Letters*, 2018, **9**, 2879–2885.

33 R. Atta-Fynn and P. Biswas, *J. Chem. Phys.*, 2018, **148**, 204503.

34 D. Beeman, J. Silverman, R. Lynds and M. R. Anderson, *Phys.Rev.B*, 1984, **30**, 870–875.

35 G. Zhao, P. Buseck, A. Rougée and M. Treacy, *Ultramicroscopy*, 2009, **109**, 177 – 188.

36 A. Filipponi, F. Evangelisti, M. Benfatto, S. Mobilio and C. R. Natoli, *Phys. Rev. B*, 1989, **40**, 9636–9643.

37 J. J. Rehr, J. J. Kas, F. D. Vila, M. P. Prange and K. Jorissen, *Phys. Chem. Chem. Phys.*, 2010, **12**, 5503–5513.

38 M. Newville, *Journal of Synchrotron Radiation*, 2001, **8**, 322–324.

39 S. Berber, Y.-K. Kwon and D. Tománek, *Phys. Rev. Lett.*, 2000, **84**, 4613–4616.

40 J. Hone, B. Batlogg, Z. Benes, A. T. Johnson and J. E. Fischer, *Science*, 2000, **289**, 1730–1733.

41 A. A. Balandin, *Nature Materials*, 2011, **10**, 569.

42 T. Zhu and E. Ertekin, *Nano Letters*, 2016, **16**, 4763–4772.

43 B. Bhattarai and D. A. Drabold, *Journal of Non-Crystalline Solids*, 2016, **439**, 6–14.

44 D. Van Tuan, A. Kumar, S. Roche, F. Ortmann, M. F. Thorpe and P. Ordejon, *Phys. Rev. B*, 2012, **86**, 121408.

45 J. M. Ziman, *Models of disorder*, Cambridge University Press, 1979.

46 S. N. Taraskin and S. R. Elliott, *Phys. Rev. B*, 1997, **56**, 8605–8622.

47 C. Chen and J. Robertson, *Journal of Non-Crystalline Solids*, 1998, **227-230**, 602–606.